Letter

Searching for the origin of the rare-earth peak with precision mass measurements across Ce–Eu isotopic chains

R. Orford,[1,2,3,*] N. Vassh,[4,†] J. A. Clark,[2,5] G. C. McLaughlin,[6] M. R. Mumpower,[7] D. Ray,[2,5] G. Savard,[2,8] R. Surman,[4] F. Buchinger,[1] D. P. Burdette,[2,4] M. T. Burkey,[2,8,‡] D. A. Gorelov,[2,5] J. W. Klimes,[2,§] W. S. Porter,[2,‖] K. S. Sharma,[5] A. A. Valverde,[2,5] L. Varriano,[2,8] and X. L. Yan[2,9]

[1]*Department of Physics, McGill University, Montréal, Québec H3A 2T8, Canada*
[2]*Physics Division, Argonne National Laboratory, Argonne, Illinois 60439, USA*
[3]*Nuclear Science Division, Lawrence Berkeley National Laboratory, Berkleley, California 94720, USA*
[4]*Department of Physics, University of Notre Dame, Notre Dame, Indiana 46556, USA*
[5]*Department of Physics and Astronomy, University of Manitoba, Winnipeg, Manitoba R3T 2N2, Canada*
[6]*Department of Physics, North Carolina State University, Raleigh, North Carolina 27695, USA*
[7]*Theoretical Division, Los Alamos National Laboratory, Los Alamos, New Mexico 87545, USA*
[8]*Department of Physics, University of Chicago, Chicago, Illinois 60637, USA*
[9]*Institute of Modern Physics, Chinese Academy of Sciences, Lanzhou 730000, China*

(Received 28 September 2021; accepted 29 March 2022; published 18 May 2022)

A nuclear mass survey of rare-earth isotopes has been conducted with the Canadian Penning Trap mass spectrometer using the most neutron-rich nuclei thus far extracted from the CARIBU facility. We present a collection of 12 nuclear masses determined with a precision of $\leqslant 10$ keV/c^2 for $Z = 58$–63 nuclei near $N = 100$. Independently, a detailed study exploring the role of nuclear masses in the formation of the r-process rare-earth abundance peak has been performed. Employing a Markov chain Monte Carlo (MCMC) technique, mass predictions of lanthanide isotopes have been made which uniquely reproduce the observed solar abundances near $A = 164$ under three distinct astrophysical outflow conditions. We demonstrate that the mass surface trends thus far mapped out by our measurements are most consistent with MCMC mass predictions given an r process that forms the rare-earth peak during an extended $(n, \gamma) \rightleftarrows (\gamma, n)$ equilibrium.

DOI: 10.1103/PhysRevC.105.L052802

With new observational data in hand [1–3], the era of multimessenger astrophysics presents promising paths toward understanding the nucleosynthesis of the heaviest elements via the rapid neutron capture process (r process). Now with the ability to probe single events, more can be said about the nature of the astrophysical sites that enriched our solar system. In order to properly analyze new observables, we must acknowledge that heavy neutron-rich nuclei, many of which have yet to be experimentally probed, put their signature on astrophysical abundances and electromagnetic transients [4–6]. Thus, it has become more pressing to exploit opportunities to address key unknown nuclear physics properties.

With recent advancements in neutron-rich nuclei production at rare isotope beam facilities [7–9], significant effort has been made to expand the landscape of nuclear physics inputs for r-process calculations, including nuclear mass measurements with improved sensitivity [10,11], half-lives of previously unobserved isotopes [12], and accurately constrained neutron capture rates [13]. In parallel with such experimental progress, advancements in machine learning methods and Bayesian techniques provide a unique opportunity to synthesize new experimental nuclear physics information and astrophysical observables. In this Letter, we demonstrate the power of such a synergy by considering the formation of the solar rare-earth abundance peak during r-process nucleosynthesis given results from a Markov chain Monte Carlo (MCMC) approach [14–16]. We report the nuclear masses of 12 neutron-rich lanthanide isotopes measured with the Canadian Penning Trap mass spectrometer (CPT) [17], including the first measurements of ^{152,153}Ce and ^{156,157}Pr. These measurements probe the most neutron-rich lanthanide masses reported to date and do so with a precision of $\leqslant 10$ keV/c^2.

To narrow in on the nuclear physics properties required for peak formation in a given type of astrophysical

*rorford@lbl.gov
†Present address: TRIUMF, 4004 Westbrook Mall, Vancouver, British Columbia V6T 2A3, Canada; nvassh@triumf.ca
‡Present address: Lawrence Livermore National Laboratory, Livermore, California 94550, USA.
§Present address: Atomic Physics Department, GSI Helmholtz Centre for Heavy Ion Research, Darmstadt 64291, Germany; Heidelberg Graduate School for Fundamental Physics, Heidelberg University, Heidelberg 69120, Germany.
‖Present address: Department of Physics, University of Notre Dame, Notre Dame, Indiana 46556, USA.

outflow, the MCMC algorithm performs mass adjustments in the neutron-rich lanthanide region and considers how well the resultant rare-earth peak abundances match observational solar data [18]. The predicted mass surfaces are intimately tied to the astrophysical outflow conditions since the required features depend on the initial *r*-process path (location of most abundant species) and the time evolution of neutron flux and density. Alongside the recent CPT mass results of Refs. [19,20], we present our new measurements along $Z = 58$–63 isotopic chains and for the first time make an extensive comparison to MCMC mass predictions given three distinct astrophysical outflows potentially found in neutron star merger environments [16]. Through such comparisons we can illuminate the dominant conditions responsible for the lanthanide element enrichment of our solar system.

The neutron-rich lanthanide masses presented in this Letter were measured with the CPT using low-energy ion beams from the Californium Rare Isotope Breeder Upgrade (CARIBU) facility [7] at Argonne National Laboratory. Each of these radioisotope ion beams originate from the spontaneously produced fission fragments of a ≈1 Ci ^{252}Cf source which were extracted from a helium-filled gas catcher at a charge state of $q = 2+$. From this continuous stream of ions, a single mass-to-charge ratio (A/q) was filtered using a pair of dipole magnets and ion bunches were then formed with a radio-frequency (rf) quadrupole cooler/buncher at a continuous rate of 10–20 Hz. They were then isochronously cycled inside the multireflection time-of-flight mass separator (MR-TOF) [21] for up to 20 ms until separation of isobaric and molecular contamination from the ions of interest was realized—routinely with mass resolving power of $R = m/\Delta m > 100\,000$. Precise mass selection was performed with a Bradbury-Nielsen gate located at the MR-TOF exit and the emerging purified bunched beam was delivered to the low-energy experimental area where further cooling was performed inside a linear Paul trap prior to injection into the CPT.

Once captured inside the Penning trap, cyclotron frequencies (ν_c) of trapped ions were measured using the phase-imaging ion-cyclotron-resonance (PI-ICR) technique [10] following the approach outlined in Ref. [22]. In this method, ν_c is calculated by measuring the accumulation of an ion's mass-dependent orbital motion while no rf excitations are applied to the Penning trap electrodes. By adjusting this excitation-free duration—the accumulation time (t_{acc})—we can probe the instantaneous phase of orbital motion by ejecting the ions from the Penning trap toward a position-sensitive microchannel plate detector (MCP) located downstream, parallel to the plane of radial motion inside the trap. A single ν_c measurement is a two-step procedure involving an initial reference phase measurement where no phase advance is permitted, followed by a final phase measurement where the mass-dependent phase advance is governed by t_{acc}. The cyclotron frequency is simply given by $\nu_c = (\phi_c + 2\pi N)/(2\pi t_{\mathrm{acc}})$, where N is the number of laps the ion completes during t_{acc} and ϕ_c represents the fractional final lap obtained by measuring the angle between the reference and final phases.

This is the opportune technique to study the most neutron-rich nuclear masses available at CARIBU, particularly in the rare-earth region where half-lives generally exceed a few hundred ms [12]. Mass resolution of up to $R \approx 25\,000\,000$ has been achieved with the CPT [23] and experimental sensitivity to measure masses of fission fragments from CARIBU with yields as low as $\approx 1 \times 10^{-5}\%$ has already been demonstrated [19].

Each CPT mass measurement begins by systematically identifying the isobars and molecular contaminants present in the beam through a series of final phase measurements with progressively higher mass resolution. Once the selected isotope's approximate ν_c is unambiguously determined, high-resolution measurements of ν_c were conducted in adherence to the established guidelines detailed in Refs. [22,24] to minimize systematic uncertainties. The most stark systematic feature in the data is due to residual magnetron motion possessed by the ions as the Penning trap measurement cycle begins. Individual ν_c measurements display a clear t_{acc} dependence described by a sinusoidal oscillation about the *true* ν_c at the frequency of magnetron motion inside the trap. Because of this effect, the true ν_c is most accurately determined by conducting several final phase measurements at accumulation times spanning ≈1 ms and fitting the data points to a simple sinusoidal model. This phenomenon and the accuracy of cyclotron frequencies inferred by this model are discussed further in Ref. [22]. Sample results from the ν_c measurement of $^{157}Pr^{2+}$ are illustrated in Fig. 1. A plot of the $t_{\mathrm{acc}} = 90.447$ ms data showing the final phase projections on the MCP is given in Fig. 1(a). In this ≈1 hour of data accumulation, 57 ions of ^{157}Pr were observed. In total, five final phase measurements were made with accumulation times ranging between 89.86 ms and 90.447 ms and the true cyclotron frequency was found from the fit shown in Fig. 1(b). Finally, masses were determined from the cyclotron frequencies of one of our reference ions, $^{82,84}Kr^{+}$ and $C_6H_6^{+}$—measured under identical experimental conditions. These are all readily available from CARIBU, have masses known with ultrahigh precision, and have A/q values similar to the ions of interest. A summary of the new CPT mass measurements are presented in Table I. Several of these masses were first reported in a 2018 Ph.D. thesis [24] and have already been incorporated into the 2020 atomic mass evaluation (AME2020) [25]. To avoid self-reference, Table I includes a comparison to values from both the AME2020 and the previous edition, AME2016 [26]. Where available, a comparison is also given between our values and previous measurements.

Our results consist of 12 neutron-rich lanthanide isotope masses including the first reported mass measurements of ^{152,153}Ce and ^{156,157}Pr. We find that each of these four masses is less bound than extrapolated values from AME2020. We also report the first Penning trap mass measurements of ^{154}Ce and ^{154}Pr. Previously, a mass excess of −52540(577) keV was determined for ^{154}Ce from the observation of six events in a storage ring [27]. This measurement was not included in AME2020 because the value was 320 keV more bound than expected from the local mass surface trend [28]. Our measured mass excess of −52068.9(24) keV is within the large uncertainty of the previous measurement and is even

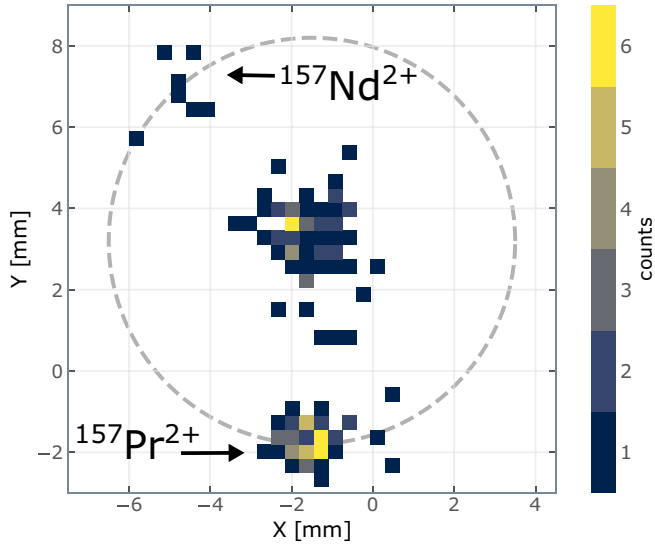

(a) An example final phase spectrum of $^{157}Pr^{2+}$

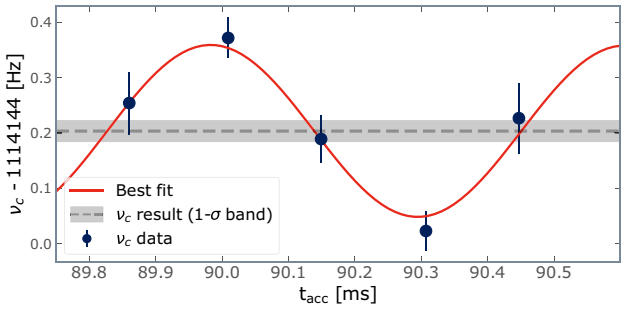

(b) Cyclotron frequency determination for $^{157}Pr^{2+}$

FIG. 1. Highlights from the ν_c measurement of $^{157}Pr^{2+}$. Panel (a) is a histogram of detected ion locations on the face of the MCP during a $t_{acc} = 90.447$ ms final phase measurement. The orbital positions of $^{157}Pr^{2+}$ and $^{157}Nd^{2+}$ ions are labeled alongside a central cluster of unexcited ions. In panel (b) the ν_c values of $^{157}Pr^{2+}$ from five distinct final phase measurements near $t_{acc} = 90$ ms are fitted to a model, described in Ref. [22], to reveal the true ν_c (gray dashed line).

less bound than the AME2020 prediction. For ^{154}Pr, the only previous mass value was derived from a single β^--endpoint energy measurement [29] and its evaluated mass had changed by 240 keV between the AME2016 and AME2020 due to a 2018 CPT mass measurement of its β^--decay daughter, ^{154}Nd [19]. Here, we have accurately established the ^{154}Pr mass for the first time with a value lying in between the two previous evaluations, reinforcing the value in measuring masses directly.

The six remaining cases in Table I (^{152,153}Pr, ^{157}Nd, ^{161}Pm, and ^{163,165}Eu) were previously studied with Penning traps using the time-of-flight ion-cyclotron-resonance technique (TOF-ICR) [30]. Evaluated masses of ^{152,153}Pr in the AME2020 are both taken from prior CPT values found in Refs. [31,32] from 2006 and 2012, respectively. Our new results for these two isotopes are more precise but for ^{153}Pr we find differences of 2.5σ and 2.1σ from the values listed in Refs. [31,32], respectively. However, the mass of ^{153}Pr from the 2012 publication is a weighted average that incorporates the prior 2006 measurement. Comparing our new value of −61547.5(24) keV directly to the raw 2012 measurement of −61540(36) keV [32], we find excellent agreement. The mass of ^{157}Nd was also first reported by the CPT in Ref. [32]. Here, we find agreement with this previous value while reducing the uncertainty from 43 keV to 2.2 keV. Finally, the masses of ^{161}Pm and ^{163,165}Eu were recently reported by JYFLTRAP [33] and in each of these cases we find consistent results. Notably, for ^{161}Pm we offer a significant factor of six improvement in precision.

We explore the implications of our neutron-rich lanthanide mass measurements from Table I alongside those from recent CPT results [19,20] by comparing to MCMC calculations which find the masses capable of forming the *r*-process rare-earth abundance peak [16]. Masses are of particular interest since they can reflect the presence of a subshell closure or nuclear deformation which make nuclei more stable than neighboring species. These features of enhanced stability influence the nuclear reaction and decay rates and make it possible for the rare-earth peak to dynamically form during nucleosynthesis. Our MCMC procedure builds such features by introducing an additional term to the mass values from a model which lacks a sufficiently strong nuclear structure feature in the lanthanide region and thus sees rare-earth abundances which are on average flat, the Duflo-Zuker (DZ) mass model [34] (see Refs. [14–16]). Our MCMC procedure is also trained to obey a few basic nuclear physics properties. Measured masses from AME2012 [35] with $140 \leqslant A \leqslant 190$ are considered in a general way by enforcing that the root-mean-square deviations from our predicted masses are no larger than they are from the DZ predictions. We impose further constraints on our mass solutions by considering the odd-even staggering of one-neutron separation energies and by taking measures to ensure that we do not introduce a feature of comparable strength to a shell closure (see Ref. [16] for details). We emphasize that the algorithm is in no way informed of the CPT mass measurements of Refs. [19,20] or of those presented in this work.

Here we consider the three distinct conditions described in Ref. [16] which are parametrized in terms of entropy (s) and dynamical timescale (τ). These outflows are all moderately neutron-rich with an electron fraction (Y_e) of 0.20. We name the three outflow conditions according to their distinct behavior: "hot" for the case in which photodissociation plays a key role at early times through $(n,\gamma) \rightleftarrows (\gamma,n)$ equilibrium and remains influential at later times, "cold" for the case that photodissociation fails to compete with neutron capture and β decay even at early times, and a "hot/cold" case with dynamics in between the two extremes that is initially determined by $(n,\gamma) \rightleftarrows (\gamma,n)$ equilibrium but follows cold dynamics at later times. All such conditions are suggested by modern simulations to take place in accretion disk winds as well as merger dynamical ejecta [36–41]. Since a distribution of outflow conditions can be found in astrophysical events, our exploration of the types of outflows which dominate solar system enrichment could be mapped back to site(s) through comparison with simulation predictions.

TABLE I. New CPT mass measurements of $Z = 58$–63 isotopes. The measured cyclotron frequency ratios ($\nu_c^{\mathrm{ref}}/\nu_c$) and mass excesses (ME) are given alongside those from AME2016 and AME2020—including nonexperimental values denoted by #. Where available, differences (Δ) from *other* directly measured mass results are noted.

			Neutral atom ME (keV)				
Ion	Reference ion	$r = \nu_c^{\mathrm{ref}}/\nu_c$	CPT	Other	Δ(CPT − other)	AME2016	AME2020
$^{152}Ce^{2+}$	$C_6H_6^+$	0.973 367 710(16)	−58878.3(23)			−58980(200)#	−58980(200)#
$^{153}Ce^{2+}$	$C_6H_6^+$	0.979 802 813(17)	−54711.5(24)			−54910(200)#	−54910(200)#
$^{154}Ce^{2+}$	$C_6H_6^+$	0.986 227 433(18)	−52068.9(24)	−52540(577)[a]	471(577)	−52220(200)#	−52220(200)#
$^{152}Pr^{2+}$	$C_6H_6^+$	0.973 333 983(69)	−63782.2(98)	−63758(19)[b]	−24(21)	−63758(19)	−63758(19)
$^{153}Pr^{2+}$	$C_6H_6^+$	0.979 755 797(17)	−61547.5(24)	−61540(36)[c]	−8(36)	−61568(12)	−61568(12)
$^{154}Pr^{2+}$	$C_6H_6^+$	0.986 186 636(18)	−58000.7(25)			−58100(110)	−57860(100)
$^{156}Pr^{2+}$	$C_6H_6^+$	0.999 044 5852(69)	−51449.2(10)			−51570(200)#	−51449.3(10)[e]
$^{157}Pr^{2+}$	$C_6H_6^+$	1.005 471 763(22)	−48434.7(32)			−48540(300)#	−48435(3)[e]
$^{157}Nd^{2+}$	$C_6H_6^+$	1.005 416 333(15)	−56494.2(22)	−56464(43)[b]	−30(43)	−56462(25)	−56494.1(2.1)[e]
$^{161}Pm^{2+}$	$^{84}Kr^+$	0.959 023 431(59)	−50086.5(92)	−50107.6(593)[d]	21(60)	−50240(300)#	−50087(9)[e]
$^{163}Eu^{2+}$	$^{82}Kr^+$	0.994 581 4612(59)	−56573.83(90)	−56575.7(38)[d]	1.9(3.9)	−56480(70)	−56573.8(9)[e]
$^{165}Eu^{2+}$	$^{84}Kr^+$	0.982 854 075(64)	−50735(10)	−50726.9(60)[d]	−8.1(11.7)	−50720(140)#	−50729(5)[e]

[a]FRS-ESR measurement, 2016 [27].
[b]CPT (TOF-ICR), 2006 [31].
[c]CPT (TOF-ICR), 2012 [32].
[d]JYFLTRAP (TOF-ICR), 2020 [33].
[e]AME2020 value contains the CPT result given here. Originally listed in a 2018 Ph.D. thesis (Ref. [24]).

In Fig. 2, we show the rare-earth abundances given the mass predictions when our MCMC procedure is applied in two distinct outflows. In both cases we are able to successfully find masses which accommodate rare-earth peak formation. These mass predictions are distinct and tied to the conditions, which is clear from considering results when the solution found in one condition is applied in the other and vice versa. Therefore comparisons between the MCMC mass solutions and mass measurements, such as those presented here, can hint at the type of outflow conditions able to accommodate both experimental and observational solar data.

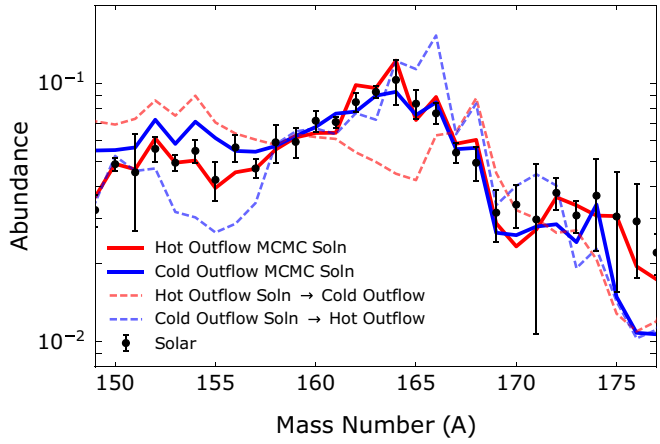

FIG. 2. Rare-earth peak abundances given the average masses predicted in Ref. [16] when two distinct astrophysical outflow conditions ("hot" in red and "cold" in blue) are considered in the MCMC calculations (solid lines). Dotted lines show results when the average masses found to produce the rare-earth peak in a given condition are applied in a distinctly different condition.

We compare our MCMC mass predictions to CPT mass measurements for six isotopic chains of rare-earth elements ($Z = 58$–63) in Fig. 3. Predictions are derived using the parallel chains method of MCMC where the average and standard deviation of 50 independent runs supplies our error estimate. Note that in the cold case predicted mass features are concentrated at $Z = 58$, as compared to the hot and hot/cold cases where features are centered at $Z = 60$, and MCMC mass adjustments fall off exponentially from the center. This means predictions several proton numbers away from 58 and 60 will mostly return to the DZ baseline. Therefore, comparisons between prediction and measurement where mass features are concentrated are of greatest importance but behavior in nearby isotopic chains can still provide valuable hints at local nuclear structure. The mass predictions found given hot outflow conditions are those which consistently match the trends in the experimental data. In the hot case, masses with $N = 102$, and particularly $N = 104$, are most important for rare-earth peak formation [16]. From examining Sm and Eu isotopic chains, we see that experiment confirms the presence of this predicted $N = 102$ behavior. In contrast, the dip in the mass surface starting at $N = 100$ predicted in both cold and hot/cold cases is not observed in any of the experimentally probed isotopic chains. However, the key features forming the rare-earth peak in cold and hot/cold cases are at $N = 108$ and $N = 106$, respectively [16]—just beyond the reach of current experiments.

Although we look forward to next-generation facilities such as the $N = 126$ factory [42] and the Facility for Rare Isotope Beams (FRIB), we have shown that our new measurements have already begun to map out potential onset of

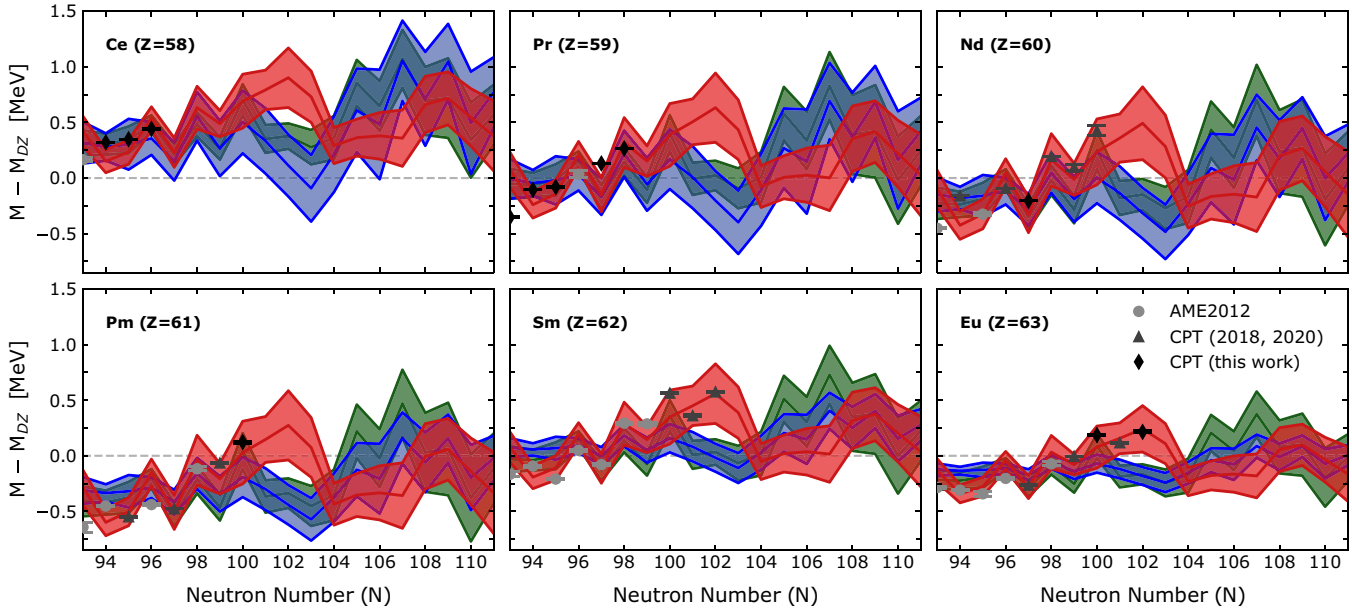

FIG. 3. Precision CPT mass measurements of neutron-rich lanthanides with $Z = 58$–63 from this work alongside Refs. [19,20] as compared to the masses predicted by the MCMC calculations of Ref. [16] (shown relative to the Duflo-Zuker mass model) given three distinct astrophysical outflow conditions: a "hot" outflow with $s = 30\ k_B$/baryon and $\tau = 70$ ms (red), a "cold" outflow with $s = 10\ k_B$/baryon and $\tau = 3$ ms (blue), and a "hot/cold" outflow with $s = 20\ k_B$/baryon and $\tau = 10$ ms (green).

key mass trend features, particularly those predicted by the hot astrophysical outflow mass solution at $N = 100$–102. We note that the framework of our MCMC calculations preserves the sensitivity that the peak formation mechanism has to the outflow conditions; therefore we cannot rule out the ability of colder conditions to be consistent with the presented mass measurements since they could form a peak from features at higher neutron numbers. Nevertheless, the overall consistency of mass prediction trends from hot conditions with measurements across six isotopic chains reinforces previous hints that hot outflows are favored [16].

Importantly, our measurements further characterize the mass surface in the neutron-rich lanthanide region where nuclear structure features consequential to the *r* process may be lurking. Several theoretical models predict different onsets of nuclear deformation in this region [43–45] (see also Fig. 6 of Ref. [46]) which in turn produces distinct trends in the mass surface [47,48]. Since nucleosynthetic outcomes are sensitive to nuclear features which enhance the stability of nuclei relative to their neighbors, mass surface trends are of critical importance in determining *r*-process abundance features such as the rare-earth peak. Therefore, since investigations of critical nuclei—such as the new Ce–Pr isotopes considered in this work—are key to mapping out lanthanide nuclear structure, our new precision mass measurements serve to constrain the nature of the lanthanide production which enriched our solar system.

This work was funded by the U.S. Department of Energy, Office of Nuclear Physics, under Awards No. DE-AC02-06CH11357 (ANL) and No. DE-AC02-05CH11231 (LBNL), and by NSERC (Canada) under Contracts No. SAPPJ-2015-00034 and No. SAPPJ-2018-00028. This research used resources of Argonne National Laboratory's ATLAS facility, which is a DOE Office of Science User Facility. The work of L.V. was supported by a National Science Foundation Graduate Research Fellowship under Grant No. DGE-1746045, and support for D.P.B. was provided by the National Science Foundation (NSF) under Grant No. PHY-1713857. The work of N.V., G.C.M., M.R.M., and R.S. was partly supported by the Fission In R-process Elements (FIRE) topical collaboration in nuclear theory, funded by the U.S. Department of Energy. Additional support was provided by the U.S. Department of Energy through Contracts No. DE-FG02-02ER41216 (G.C.M.), No. DE-FG02-95-ER40934 (R.S.), and No. DE-SC0018232 (SciDAC TEAMS collaboration, R.S.). R.S. and G.C.M. also acknowledge support by the National Science Foundation N3AS Hub Grant No. PHY-1630782 and Physics Frontiers Center No. PHY-2020275. M.R.M. was supported by the U.S. Department of Energy through the Los Alamos National Laboratory. Los Alamos National Laboratory is operated by Triad National Security, LLC, for the National Nuclear Security Administration of the U.S. Department of Energy (Contract No. 89233218CNA000001). This work was partially enabled by the National Science Foundation under Grant No. PHY-1430152 (JINA Center for the Evolution of the Elements). This work utilized the computational resources of the Laboratory Computing Resource Center at Argonne National Laboratory (ANL LCRC) and the University of Notre Dame Center for Research Computing (ND CRC). We specifically acknowledge the assistance of Stanislav Sergienko (ANL LCRC) and Scott Hampton (ND CRC). This manuscript has been released via Los Alamos National Laboratory Report No. LA-UR-21-30295.

[1] B. P. Abbott *et al.* (LIGO Scientific Collaboration and Virgo Collaboration), Phys. Rev. Lett. **119**, 161101 (2017).

[2] S. J. Smartt *et al.*, Nature (London) **551**, 75 (2017).

[3] D. Watson, C. J. Hansen, J. Selsing *et al.*, Nature (London) **574**, 497 (2019).

[4] B. Côté, C. L. Fryer, K. Belczynski, O. Korobkin, M. Chruślińska, N. Vassh, M. R. Mumpower, J. Lippuner, T. M. Sprouse, R. Surman, and R. Wollaeger, Astrophys. J. **855**, 99 (2018).

[5] Y. L. Zhu, K. A. Lund, J. Barnes, T. M. Sprouse, N. Vassh, G. C. McLaughlin, M. R. Mumpower, and R. Surman, Astrophys. J. **906**, 94 (2021).

[6] X. Wang, N3AS Collaboration, N. Vassh, FIRE Collaboration, T. Sprouse, M. Mumpower, R. Vogt, J. Randrup, and R. Surman, Astrophys. J. Lett. **903**, L3 (2020).

[7] G. Savard, S. Baker, C. Davids, A. Levand, E. Moore, R. Pardo, R. Vondrasek, B. Zabransky, and G. Zinkann, Nucl. Instrum. Methods Phys. Res., Sect. B **266**, 4086 (2008).

[8] T. Kubo, Nucl. Instrum. Methods Phys. Res., Sect. B **204**, 97 (2003).

[9] I. D. Moore *et al.*, Nucl. Instrum. Methods Phys. Res., Sect. B **317**, 208 (2013).

[10] S. Eliseev, K. Blaum, M. Block, C. Droese, M. Goncharov, E. Minaya Ramirez, D. A. Nesterenko, Y. N. Novikov, and L. Schweikhard, Phys. Rev. Lett. **110**, 082501 (2013).

[11] R. N. Wolf, F. Wienholtz, D. Atanasov, D. Beck, K. Blaum, C. Borgmann, F. Herfurth, M. Kowalska, S. Kreim, Y. A. Litvinov, D. Lunney, V. Manea, D. Neidherr, M. Rosenbusch, L. Schweikhard, J. Stanja, and K. Zuber, Int. J. Mass Spectrom. **349-350**, 123 (2013).

[12] J. Wu *et al.*, Phys. Rev. Lett. **118**, 072701 (2017).

[13] A. Spyrou, S. N. Liddick, A. C. Larsen, M. Guttormsen, K. Cooper, A. C. Dombos, D. J. Morrissey, F. Naqvi, G. Perdikakis, S. J. Quinn, T. Renstrøm, J. A. Rodriguez, A. Simon, C. S. Sumithrarachchi, and R. G. T. Zegers, Phys. Rev. Lett. **113**, 232502 (2014).

[14] M. R. Mumpower, G. C. McLaughlin, R. Surman, and A. W. Steiner, Astrophys. J. **833**, 282 (2016).

[15] M. R. Mumpower, G. C. McLaughlin, R. Surman, and A. W. Steiner, J. Phys. G: Nucl. Part. Phys. **44**, 034003 (2017).

[16] N. Vassh, G. C. McLaughlin, M. R. Mumpower, and R. Surman, Astrophys. J. **907**, 98 (2021).

[17] J. Van Schelt, D. Lascar, G. Savard, J. A. Clark, P. F. Bertone, S. Caldwell, A. Chaudhuri, A. F. Levand, G. Li, G. E. Morgan, R. Orford, R. E. Segel, K. S. Sharma, and M. G. Sternberg, Phys. Rev. Lett. **111**, 061102 (2013).

[18] S. Goriely, Astron. Astrophys. **342**, 881 (1999).

[19] R. Orford, N. Vassh, J. A. Clark, G. C. McLaughlin, M. R. Mumpower, G. Savard, R. Surman, A. Aprahamian, F. Buchinger, M. T. Burkey, D. A. Gorelov, T. Y. Hirsh, J. W. Klimes, G. E. Morgan, A. Nystrom, and K. S. Sharma, Phys. Rev. Lett. **120**, 262702 (2018).

[20] R. Orford, F. G. Kondev, G. Savard, J. A. Clark, W. S. Porter, D. Ray, F. Buchinger, M. T. Burkey, D. A. Gorelov, D. J. Hartley, J. W. Klimes, K. S. Sharma, A. A. Valverde, and X. L. Yan, Phys. Rev. C **102**, 011303(R) (2020).

[21] T. Y. Hirsh *et al.*, Nucl. Instrum. Methods Phys. Res., Sect. B **376**, 229 (2016).

[22] R. Orford, J. A. Clark, G. Savard, A. Aprahamian, F. Buchinger, M. T. Burkey, D. A. Gorelov, J. W. Klimes, G. E. Morgan, A. Nystrom, W. S. Porter, D. Ray, and K. S. Sharma, Nucl. Instrum. Methods Phys. Res., Sect. B **463**, 491 (2020).

[23] A. J. Mitchell, R. Orford, G. J. Lane, C. J. Lister, P. Copp, J. A. Clark, G. Savard, J. M. Allmond, A. D. Ayangeakaa, S. Bottoni, M. P. Carpenter, P. Chowdhury, D. A. Gorelov, R. V. F. Janssens, F. G. Kondev, U. Patel, D. Seweryniak, M. L. Smith, Y. Y. Zhong, and S. Zhu, Phys. Rev. C **103**, 024323 (2021).

[24] R. Orford, A phase-imaging technique for precision mass measurements of neutron-rich nuclei with the Canadian Penning Trap mass spectrometer, Ph.D. thesis, McGill University, 2018.

[25] M. Wang, H. Huang, F. Kondev, G. Audi, and S. Naimi, Chin. Phys. C **45**, 030003 (2021).

[26] M. Wang, G. Audi, F.G. Kondev, W.J. Huang, S. Naimi, and X. Xu, Chin. Phys. C **41**, 030003 (2017).

[27] R. Knöbel *et al.*, Eur. Phys. J. A **52**, 138 (2016).

[28] W. J. Huang, M. Wang, F. G. Kondev, G. Audi, and S. Naimi, Chin. Phys. C **45**, 030002 (2021).

[29] M. Shibata, T. Shindou, K. Kawade, Y. Kojima, A. Taniguchi, Y. Kawase, and S. Ichikawa, in *Exotic Nuclei and Atomic Masses* (Springer, Berlin, 2003), p. 479.

[30] M. König, G. Bollen, H.-J. Kluge, T. Otto, and J. Szerypo, Int. J. Mass Spectrom. Ion Processes **142**, 95 (1995).

[31] G. Savard *et al.*, Int. J. Mass Spectrom. **251**, 252 (2006).

[32] J. Van Schelt, D. Lascar, G. Savard, J. A. Clark, S. Caldwell, A. Chaudhuri, J. Fallis, J. P. Greene, A. F. Levand, G. Li, K. S. Sharma, M. G. Sternberg, T. Sun, and B. J. Zabransky, Phys. Rev. C **85**, 045805 (2012).

[33] M. Vilen, J. M. Kelly, A. Kankainen, M. Brodeur, A. Aprahamian, L. Canete, R. P. de Groote, A. de Roubin, T. Eronen, A. Jokinen, I. D. Moore, M. R. Mumpower, D. A. Nesterenko, J. O'Brien, A. P. Perdomo, H. Penttilä, M. Reponen, S. Rinta-Antila, and R. Surman, Phys. Rev. C **101**, 034312 (2020).

[34] J. Duflo and A. P. Zuker, Phys. Rev. C **52**, R23 (1995).

[35] G. Audi, M. Wang, A. H. Wapstra, F. G. Kondev, M. MacCormick, X. Xu, and B. Pfeiffer, Chin. Phys. C **36**, 1287 (2012).

[36] R. Surman, G. C. McLaughlin, M. Ruffert, H. T. Janka, and W. R. Hix, Astrophys. J. **679**, L117 (2008).

[37] B. D. Metzger, T. A. Thompson, and E. Quataert, Astrophys. J. **676**, 1130 (2008).

[38] A. Perego, S. Rosswog, R. M. Cabezón, O. Korobkin, R. Käppeli, A. Arcones, and M. Liebendörfer, Mon. Not. R. Astron. Soc. **443**, 3134 (2014).

[39] R. Fernández, D. Kasen, B. D. Metzger, and E. Quataert, Mon. Not. R. Astron. Soc. **446**, 750 (2015).

[40] O. Just, A. Bauswein, R. A. Pulpillo, S. Goriely, and H.-T. Janka, Mon. Not. R. Astron. Soc. **448**, 541 (2015).

[41] D. Radice, A. Perego, K. Hotokezaka, S. A. Fromm, S. Bernuzzi, and L. F. Roberts, Astrophys. J. **869**, 130 (2018).

[42] G. Savard, M. Brodeur, J. A. Clark, R. A. Knaack, and A. A. Valverde, Nucl. Instrum. Methods Phys. Res., Sect. B **463**, 258 (2020).

[43] J. Bartel, P. Quentin, M. Brack, C. Guet, and H. B. Håkansson, Nucl. Phys. A **386**, 79 (1982).

[44] E. Chabanat, P. Bonche, P. Haensel, J. Meyer, and R. Schaeffer, Nucl. Phys. A **635**, 231 (1998).

[45] M. Kortelainen, T. Lesinski, J. Moré, W. Nazarewicz, J. Sarich, N. Schunck, M. V. Stoitsov, and S. Wild, Phys. Rev. C **82**, 024313 (2010).

[46] C. J. Horowitz *et al.*, J. Phys. G: Nucl. Part. Phys. **46**, 083001 (2019).

[47] J. Terasaki, H. Flocard, P. H. Heenen, and P. Bonche, Nucl. Phys. A **621**, 706 (1997).

[48] A. de Roubin, D. Atanasov, K. Blaum, S. George, F. Herfurth, D. Kisler, M. Kowalska, S. Kreim, D. Lunney, V. Manea, E. Minaya Ramirez, M. Mougeot, D. Neidherr, M. Rosenbusch, L. Schweikhard, A. Welker, F. Wienholtz, R. N. Wolf, and K. Zuber, Phys. Rev. C **96**, 014310 (2017).